k-t BLAST Reconstruction From Non-Cartesian *k-t* Space Sampling

Michael S. Hansen,[1,2*] Christof Baltes,[1] Jeffrey Tsao,[3] Sebastian Kozerke,[1] Klaas P. Pruessmann,[1] and Holger Eggers[4]

Current implementations of *k-t* Broad-use Linear Acqusition Speed-up Technique (BLAST) require the sampling in *k-t* space to conform to a lattice. To permit the use of *k-t* BLAST with non-Cartesian sampling, an iterative reconstruction approach is proposed in this work. This method, which is based on the conjugate gradient (CG) method and gridding reconstruction principles, can efficiently handle data that are sampled along non-Cartesian trajectories in *k-t* space. The approach is demonstrated on prospectively gated radial and retrospectively gated Cartesian imaging. Compared to a sliding window (SW) reconstruction, the resulting image series exhibit lower artifact levels and improved temporal fidelity. The proposed approach thus allows investigators to combine the specific advantages of non-Cartesian imaging or retrospective gating with the acceleration provided by *k-t* BLAST. Magn Reson Med 55: 85–91, 2006. © 2005 Wiley-Liss, Inc.

Key words: dynamic imaging; *k-t* BLAST; image reconstruction; iterative reconstruction; retrospective gating; radial imaging

To achieve faster dynamic imaging, *k*-space is often undersampled, and accordingly there is great interest in reconstruction methods that are able to cope with the resulting aliasing. Fortunately, image series of naturally occurring objects show considerable correlation in space and time, and hence permit an approximation with fewer degrees of freedom compared to a full sampling of *k*-space for each time point. This aspect is being exploited by a number of new fast dynamic imaging techniques, such as unaliasing by Fourier-encoding the overlaps using the temporal dimension (UNFOLD) (1), *k-t* Broad-use Linear Acquisition Speed-up Technique (BLAST) (2), temporal sensitivity encoding (TSENSE) (3), and *k-t* SENSE (2).

These techniques accelerate the imaging by skipping the acquisition of certain data. This undersampling leads to aliasing, which is removed by adaptive temporal filtering based on general assumptions about the imaged object (UNFOLD), adaptive filtering incorporating explicit prior information about the imaged object (*k-t* BLAST), coil sensitivity encoding with temporal filtering for residual aliasing reduction (TSENSE), or a combination of coil sensitivity encoding and *k-t* BLAST (*k-t* SENSE). For all of these techniques, the reconstruction is considerably simplified by restricting the sampling to a sheared grid (or lattice) in *k-t* space (*k* is the spatial frequency, and *t* is the temporal dimension), because this causes the aliasing to also be confined to a lattice in the corresponding *x-f* space (*x* is the spatial dimension, and *f* is the temporal frequency) (4–6). The point spread function (PSF) in *x-f* space simply becomes a set of δ-functions, and the aliasing can be resolved separately for small sets of points in *x-f* space, thus allowing a substantially faster reconstruction. Therefore, to date the above-mentioned dynamic imaging techniques have been applied mainly to acquisition methods that sample *k-t* space on a lattice.

Although the condition of lattice sampling is often met, a number of relevant and useful acquisition methods are excluded by it. One example is radial imaging. The more complicated PSF makes radial acquisitions unsuitable for the simplified reconstruction, but since trajectories with circular symmetry have inherent advantages for motion they are interesting for dynamic studies. In *k-t* BLAST there is the additional advantage that the training data are readily available from the densely sampled center of *k*-space. Another example is acquisition using retrospective cardiac gating (7). Such acquisitions are also difficult to adapt to the simplified reconstruction because the precise timing (with respect to the length of the cardiac cycle) of each individual *k*-space profile is unknown at the time of acquisition. In this case, the resulting PSF depends both on heart rate variations and the undersampling strategy used.

Examples of non-Cartesian *k*-space sampling and temporal processing have been presented. UNFOLD has been used in conjunction with spiral sampling (1), but only for cases in which the dynamics of the object occur at a single known frequency. This simplified assumption entails that the reconstruction involves only gridding followed by filtering, and it does not involve actually solving the inverse problem. Similarly, undersampled radial imaging has been used with low-pass filtering in the temporal direction (i.e., sliding window (SW)) to reduce the streaking artifacts (8). In another approach, finite support constraint is used to remove streaking artifacts in undersampled radial imaging (10). The *k-t* BLAST method, which is the focus of this paper, has also been used in non-Cartesian (radial) imaging, but only using an approximation in the reconstruction procedure (11). Common to all of these examples is the fact that they either do not solve the inverse problem or the inverse problem is simplified (e.g., Ref. 10). In this paper we present a method for solving the inverse problem in a practical way.

[1]Institute for Biomedical Engineering, Swiss Federal Institute of Technology (ETH), Zurich, Switzerland.

[2]MR Center, Skejby Hospital, Aarhus University Hospital, Denmark.

[3]Novartis Institutes of BioMedical Research, Inc., Cambridge, Massachusetts, USA.

[4]Philips Research Laboratories, Hamburg, Germany.

Grant sponsor: Danish Heart Foundation; Grant number: 02-2-3-43-22021.

*Correspondence to: Michael Schacht Hansen, MR Center, Skejby Hospital, Brendstrupgaardsvej, DK-8200 Aarhus N, Denmark. E-mail: msh@mr.au.dk

Received 2 June 2005; revised 22 August 2005; accepted 23 August 2005.
DOI 10.1002/mrm.20734
Published online 1 December 2005 in Wiley InterScience (www.interscience.wiley.com).

The original paper on *k-t* BLAST and *k-t* SENSE (2) described mathematically how to reconstruct image series from an non-Cartesian sampling of *k-t* space. The reconstruction involves an inversion, which is impractical to solve with direct methods. An iterative approach was therefore suggested. However, to date it has not been demonstrated in practice.

A related problem is encountered when the parallel imaging technique SENSE (12) is applied to non-Cartesian *k*-space sampling. It has been shown that an efficient reconstruction is possible in this case with the use of an iterative approach that relies on the conjugate gradient (CG) method and gridding reconstruction principles (13). In this work we propose to use a similar approach to solve the inverse problem that arises in *k-t* BLAST with non-Cartesian *k-t* space sampling, and we demonstrate its feasibility with two applications: 1) radial *k*-space sampling and 2) Cartesian *k*-space sampling with retrospective cardiac gating. In addition, we explore the impact of different sampling strategies for the retrospective cardiac gating application. This serves to illustrate the fact that although reconstruction from arbitrary sampling schemes is possible, the sampling strategy has a profound impact on the reconstruction result.

MATERIALS AND METHODS

Reconstruction

The *k-t* BLAST reconstruction is described by (2):

$$\boldsymbol{\rho}_{x,f} = (\mathbf{E}^{\mathrm{H}}\boldsymbol{\Psi}_{k,t}^{-1}\mathbf{E} + \boldsymbol{\Theta}_{x,f}^{-1})^{+}\mathbf{E}^{\mathrm{H}}\boldsymbol{\Psi}_{k,t}^{-1}\mathbf{d}_{k,t}. \quad [1]$$

In this equation the encoding matrix $\mathbf{E}$ is defined as $\mathbf{E} = [\Xi_{k,t}\mathrm{FT}_{xf\rightarrow kt}]$ where $\mathrm{FT}_{xf\rightarrow kt}$ denotes Fourier transformation from *x-f* space to *k-t* space, and $\Xi_{k,t}$ denotes the sampling onto an non-Cartesian trajectory. $\boldsymbol{\Theta}_{x,f}$ is the signal covariance matrix $\langle\boldsymbol{\rho}_{x,f}\cdot\boldsymbol{\rho}_{x,f}^{\mathrm{H}}\rangle$, $\boldsymbol{\Psi}_{k,t}$ is the noise covariance matrix, and $\mathbf{d}_{k,t}$ and $\boldsymbol{\rho}_{x,f}$ are vectors containing the measured data points in *k-t* space and the unaliased reconstructed signal in *x-f* space, respectively. Superscript H indicates the complex conjugate transpose, and superscript + indicates the Moore-Penrose pseudo-inverse.

The signal covariance matrix $\boldsymbol{\Theta}_{x,f}$ is generally not available, but estimates of its diagonal elements can be obtained rather easily from a low-spatial-resolution training data set. Consequently, $\boldsymbol{\Theta}_{x,f}$ is approximated with a diagonal matrix $\mathbf{M}_{x,f}^2$ containing only the squared estimated signal intensities from the training acquisition (i.e., the estimated signal variance). This approximation has some important consequences. First, off-diagonal elements of the signal covariance matrix are set to zero. This adds to the stability of the reconstruction, but it also limits the accuracy with which the signal distribution can be recovered. Second, since the diagonal elements are estimated from low-spatial-resolution data, they will have limited accuracy, which will influence the reconstruction. In general, if the diagonal elements are underestimated, this will lead to too much filtering in *x-f* space and usually to temporal blurring. If the diagonal elements are overestimated, residual aliasing will be present in the reconstruction. Furthermore, it is assumed that the noise is uncorrelated and uniform in *k-t* space. Thus, Eq. [1] simplifies to:

$$\boldsymbol{\rho}_{x,f} = (\mathbf{E}^{\mathrm{H}}\boldsymbol{\sigma}_{k,t}^{-2}\mathbf{E} + \mathbf{M}_{x,f}^{-2})^{+}\mathbf{E}^{\mathrm{H}}\boldsymbol{\sigma}_{k,t}^{-2}\mathbf{d}_{k,t}, \quad [2]$$

where $\sigma_{k,t}^2$ is the noise variance.

The objective of a general implementation of the *k-t* BLAST reconstruction is to evaluate Eq. [2] for any $\mathbf{E}$. However, the size of the system matrix ($\mathbf{E}^{\mathrm{H}}\boldsymbol{\sigma}_{k,t}^{-2}\mathbf{E} + \mathbf{M}_{x,f}^{-2}$) makes the explicit calculation of its pseudo-inverse impractical. Thus, it is preferable to use an iterative approach instead. The CG method (14) was chosen for this work because it has successfully been applied to a related problem arising in non-Cartesian SENSE imaging (15). In each iteration step, it requires the multiplication of a search vector by the system matrix. Normally, even the evaluation of this product is computationally demanding, but the use of gridding reconstruction principles, as suggested in Ref. 15, allows the complexity to be reduced to a tolerable level. Specifically, since $\mathbf{E}$ contains only Fourier terms, multiplications with $\mathbf{E}$ and $\mathbf{E}^{\mathrm{H}}$ can be replaced with a gridding operation and FFT.

The speed of convergence of the CG method depends on the condition of the system matrix. Preconditioning of the system matrix is desirable to improve conditioning and achieve satisfactory convergence within a tolerable number of iterations. The system matrix of Eq. [2] lends itself well to a simple preconditioning with a diagonal matrix $\mathbf{D}$:

$$\mathbf{D}(\mathbf{E}^{\mathrm{H}}\boldsymbol{\sigma}_{k,t}^{-2}\mathbf{E} + \mathbf{M}_{x,f}^{-2})\mathbf{D}(\mathbf{D}^{-1}\boldsymbol{\rho}_{x,f}) = \mathbf{D}\mathbf{E}^{\mathrm{H}}\boldsymbol{\sigma}_{k,t}^{-2}\mathbf{d}_{k,t}. \quad [3]$$

This diagonal matrix $\mathbf{D}$, with elements d_{ii}, aims to equalize the diagonal elements of the system matrix (16), which is accomplished by choosing

$$\mathrm{d}_{\mathrm{ii}} = \frac{1}{\sqrt{(\mathbf{E}^{\mathrm{H}}\boldsymbol{\sigma}_{k,t}^{-2}\mathbf{E} + \mathbf{M}_{x,f}^{-2})_{ii}}} = \frac{1}{\sqrt{\mathrm{N}/\sigma_{k,t}^2 + 1/\mathrm{m}_{ii}^2}}, \quad [4]$$

where N is the number of elements being Fourier transformed, and m_{ii}^2 is the ith diagonal element of $\mathbf{M}_{x,f}^2$

A comparison of Eqs. [2] and [3] shows that the preconditioning does not alter the solution, since the equation to be solved remains the same. Specifically, the purpose of the preconditioning is separate from the purpose of the training data scan, although the training data is used to estimate the preconditioning matrix in this case. Even if a wrong precondition matrix is used, it will not affect the result. It only modifies the convergence rate.

Consequently, the proposed reconstruction involves solving Eq. [3] with the CG method. The details of the implementation can be found in Fig. 1. Briefly, the iteration starts by assuming that the solution is a vector of zeros (i.e., no initial guess). This starting vector is then iteratively improved by applying the system matrix to search vectors. The multiplication of the system matrix and the search vector is made efficient with the use of gridding reconstruction principles. It was implemented in Matlab R13 (The MathWorks, Inc., Natick, MA, USA) running on standard PC hardware.

The necessary training data ($\mathbf{M}_{x,f}^2$) may be extracted directly from the undersampled imaging data if the sampling in the center of *k*-space is dense enough. For example, in the case of moderately undersampled radial imaging, a sufficiently large region in the center of *k*-space is fully sampled. A *k*-space shutter can be applied to extract this

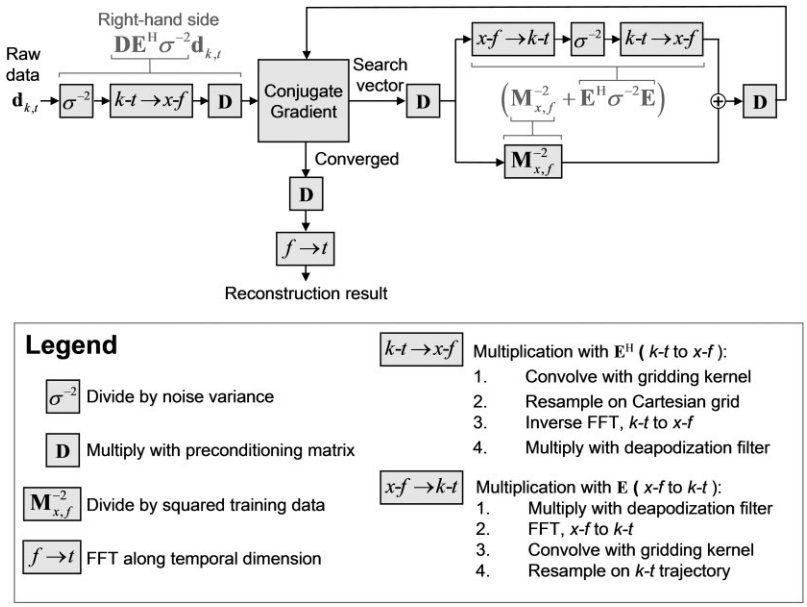

FIG. 1. Implementation of the reconstruction. The CG method solves the system of linear equations defined in Eq. [3]. First, the right-hand side of the equation is formed and fed into the CG iteration. In each iteration step a search vector is multiplied with the system matrix. The multiplications with **E** and $\mathbf{E}^{\mathrm{H}}$ are approximated with gridding reconstruction principles as indicated. It is possible (but not necessary) to include sampling density compensation in the gridding routines. This generally lowers the required number of iterations. The result and the remaining residual are then used to update the search and the solution vectors. The mentioned gridding operations are only performed along dimensions that are nonuniformly sampled. The procedure continues until either the residual has fallen below a certain level or a fixed number of iterations have been completed. In the present implementation, no starting image (initial guess) is used for the CG method.

region, and the signal variance estimates needed in the iterative reconstruction can be obtained by gridding reconstruction.

Radial Imaging

A data set with 25 cardiac phases was acquired with prospective ECG gating in a healthy volunteer. A Philips Intera 1.5T whole-body scanner (Philips Medical Systems, Best, The Netherlands), a five-element phased-array receive coil, and a steady-state free precession (SSFP) sequence were used. The matrix size was 176×176, the field of view (FOV) was 440×440 mm^2, the TR was 3.1 ms, the TE was 1.6 ms, and the bandwidth was 1136 Hz per pixel. A total of 208 projections were collected for each cardiac phase, which corresponds to 25% undersampling compared to the Nyquist limit of $\pi/2 \cdot 176 \approx 277$ projections. It is usually acceptable to use moderate undersampling in radial imaging, because of the relatively benign nature of the resulting aliasing artifacts (17). Therefore, in the following text the data set with 208 projections is referred to as "fully sampled."

This data set was used to generate undersampled data sets for *k-t* BLAST reconstruction by selecting a subset of the collected projections. Data sets with 52 and 26 projections (four- and eightfold undersampling) per frame were generated such that the sampling pattern rotated by one projection with each frame (e.g., for fourfold acceleration, frame 1 contained projections [1, 5, 9, . . ., 205], frame 2 contained projections [2, 6, 10, . . ., 206], etc.). The fully sampled central part of the *k*-space was extracted and used as training data for *k-t* BLAST reconstruction. A *k*-space shutter with a diameter of 1/4 and 1/8 of the matrix size was used for four- and eightfold acceleration, respectively. As in all of the following experiments, the reconstruction was performed separately for each receive coil, and the results were subsequently combined using the root-mean-square (RMS) method (18). The images were compared with those reconstructed from the fully sampled data set both visually and in terms of RMS reconstruction error as described in Ref. 19.

Retrospective Cardiac Gating

In retrospectively gated cardiac acquisitions, *k*-space profiles are acquired continuously while the ECG signal is monitored. Each acquired profile is then assigned a relative time within the cardiac cycle after the ECG signal is evaluated. Specifically, each monitored cardiac cycle undergoes stretching or shrinking (normalization) to fit an average cardiac cycle. A time point is then assigned to the acquired profiles with respect to this average cardiac cycle. In this work we used a simple nonlinear normalization that takes into account the fact that variations in the R-R interval usually affect the diastole most, while the length of the systole remains more or less constant.

A fully sampled, retrospectively gated data set was acquired in a healthy volunteer in a Philips Intera 1.5T whole-body scanner using a five-element phased-array receive coil. An SSFP sequence with a TR of 3.9 ms and a TE of 1.9 ms was used. The scan matrix was 192×150, the FOV was 300×238 mm^2, and the bandwidth was 724 Hz per pixel. A total of 4580 *k*-space profiles were acquired evenly distributed over the cardiac cycle. There were sufficient data to reconstruct 30 cardiac phases. The data were acquired as illustrated in the upper left corner of Fig. 2, which is based on actual timing information from an in vivo acquisition. The acquisition is divided into target R-R intervals (marked with "R-R interval") using the average cardiac frequency entered by the user. In each of these target R-R intervals, a set of *k*-space profiles is repeatedly acquired to cover the entire cardiac cycle. A new set of profiles is acquired in each following target R-R interval. This strategy results in a PSF which is close to a δ-function, as seen in the upper right corner of Fig. 2.

Two possible approaches for undersampling were tested by subsampling this data set. The first approach, illustrated in the middle row of Fig. 2, was designed to be as

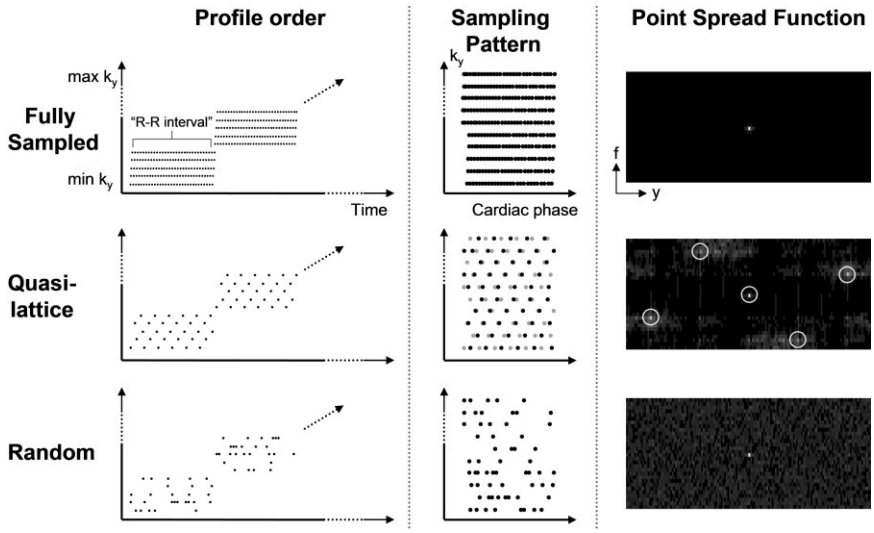

FIG. 2. Sampling strategies for retrospectively gated Cartesian imaging. The first row shows the typical sampling strategy for a full acquisition. The measurement is grouped into target "R-R intervals," in which a certain number of profiles are acquired repeatedly (i.e., the same profiles are sampled for different target cardiac phases). Ideally, *k*-space is uniformly covered for all cardiac phases, and the resulting PSF is very close to a δ-function. Two possible strategies for an undersampled acquisition are proposed in the two lower rows. The first, called "quasi-lattice," aims to be as close to lattice sampling as possible. The sampling pattern (black dots) is similar to a lattice (gray dots), and the PSF shows five distinct main lobes. However, these main lobes are not as well defined, because they are in a prospectively gated acquisition. The locations where the five δ-functions would be in the ideal case are marked with white circles. In contrast, the second strategy, called "random," leads to a PSF with only one distinct main lobe, and the rest of the aliasing is spread diffusely.

close to lattice sampling (4,5) as possible, i.e., it would result in sampling on a sheared grid in *k-t* space if the cardiac frequency of the subject was identical to the target frequency throughout the acquisition. Optimal sampling patterns, as described in Ref. 20, were used to extract undersampled data sets for five- and eightfold acceleration. An example of the resulting profile order, *k-t* sampling pattern, and PSF for fivefold acceleration is shown in the middle row of Fig. 2. Note that there are quite large deviations in the exact location of the samples, but that the overall appearance of the pattern still resembles the optimal sheared grid. The PSF still has five distinct main lobes, but they are no longer δ-functions, and the aliasing pattern becomes more complicated. The second approach involved random undersampling, which has the advantage that the aliasing becomes more diffuse and noise-like (21). An example of the resulting profile order, *k-t* sampling pattern, and PSF is provided in the lower row of Fig. 2. The PSF has only one distinct main lobe now, and the aliasing is being distributed in a more random fashion. A potential disadvantage of this approach is that overlaps among signal-bearing regions are guaranteed to occur.

The acquisition of the training data is not illustrated in Fig. 2. It could, however, be integrated into both of the suggested undersampling strategies straightforwardly (i.e., the acquisition could switch from undersampling to full sampling for the center of *k*-space). Alternatively, the training data may be acquired in a separate acquisition.

In this work the central 12 profiles of the fully sampled data set were used as low-resolution training data. This choice was based on previous results (19). Thus, the net acceleration was 3.7 and 5.1 for five- and eightfold acceleration, respectively. *k-t* BLAST reconstructions were compared with SW reconstructions in terms of the RMS reconstruction error. In the *k-t* BLAST reconstruction, the interpolation along time was handled exactly as that in *k*-space in the radial experiments described above. The sliding window reconstruction was implemented as a convolution along time with a triangular window. The latter was implemented as a convolution along time with a triangular window. The width of this window was equal to the acceleration factor except that it was expanded, if no samples fell within the window's support at a given *k*-space location and time. A normalization of the weights within each window was used to compensate for the variations in sampling density.

CG Stopping Criteria

To investigate the convergence behavior of the proposed reconstruction, an initial experiment based on fully sampled data sets was conducted. Prospectively gated radial and retrospectively gated Cartesian acquisitions were undersampled to an acceleration factor of 8, as described above. The residual (i.e., the 2-norm of the residuum vector) and the mean RMS reconstruction error over all cardiac phases were monitored over several iterations. The result of this is seen in Fig. 3. Within the first 10 iterations the residual dropped to less than 0.1% in both cases. At the same time the RMS reconstruction error stabilized and there was no further improvement in the reconstruction. This observation is based on the fact that the improvements in reconstruction quality beyond this point are below the noise level. Based on this finding, we chose to let the iteration run for 10 iterations in all experiments presented here. It took approximately 3 min to perform 10 iterations for a single receive coil.

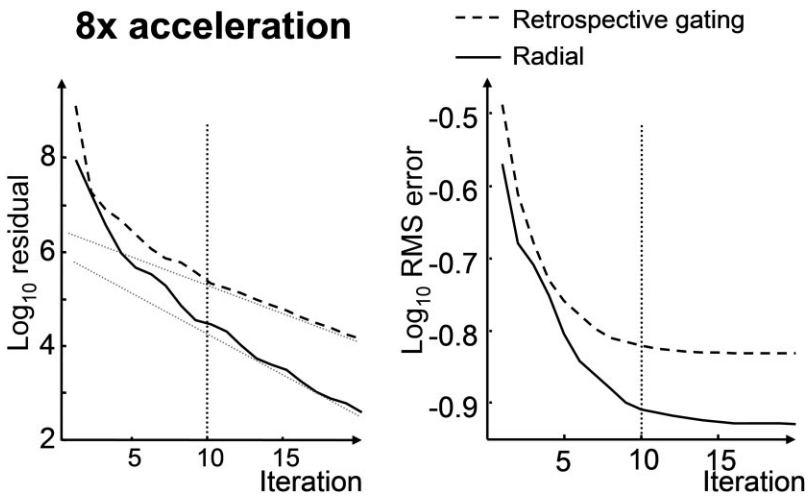

FIG. 3. Analysis of convergence. Results are shown for retrospectively gated Cartesian (random undersampling) and prospectively gated radial imaging, both with eightfold acceleration. The left panel and right panels depict the decrease of the residual and the RMS reconstruction error, respectively. The decrease of the residual is very rapid during the first iterations and then becomes exponential. The RMS reconstruction error shows no further substantial improvement after about 10 iterations (indicated by a vertical dotted line).

RESULTS

Radial Imaging

Figure 4 shows the radial results. An *x-t* plot from a position passing through the left ventricle (LV) is provided for each reconstruction result. The *x-t* plots illustrate that the *k-t* BLAST reconstructions capture the motion of the LV well, whereas the SW reconstruction suffers from temporal blurring. This is confirmed by the RMS reconstruction error plotted on the right of Fig. 4. The SW reconstructions show a particular increase in reconstruction error in frames acquired around late systole, as marked by the arrows. Furthermore, the SW reconstruction has an increased reconstruction error compared to *k-t* BLAST in all other cardiac phases, albeit by a smaller amount.

Retrospective Cardiac Gating

The RMS reconstruction errors for the two undersampling strategies are given in Fig. 5. The *k-t* BLAST reconstruction shows lower errors than the SW reconstruction in all cases. Even *k-t* BLAST at eightfold undersampling is better than the SW reconstruction at fivefold undersampling. The quasi-lattice sampling performs better than the random sampling in both *k-t* BLAST and SW reconstruction.

Figure 6 illustrates the artifacts that arise from SW reconstruction. Compared to the results for full sampling, the *k-t* BLAST reconstructions have few artifacts, whereas the SW reconstructions have some residual aliasing emanating from the contracting LV. There is also less temporal blurring of the LV in the *k-t* BLAST reconstructions.

DISCUSSION AND CONCLUSIONS

This paper demonstrates the feasibility of performing *k-t* BLAST reconstruction from data acquired on non-Cartesian trajectories in *k-t* space. The reconstruction requires solving a very large linear system of equations, which makes it prohibitively time-consuming to invert it directly. Alternatively, the inverse problem can be solved iteratively. The proposed combination of CG method and gridding reconstruction principles reduces the computational time of the reconstruction to a few minutes per receive coil.

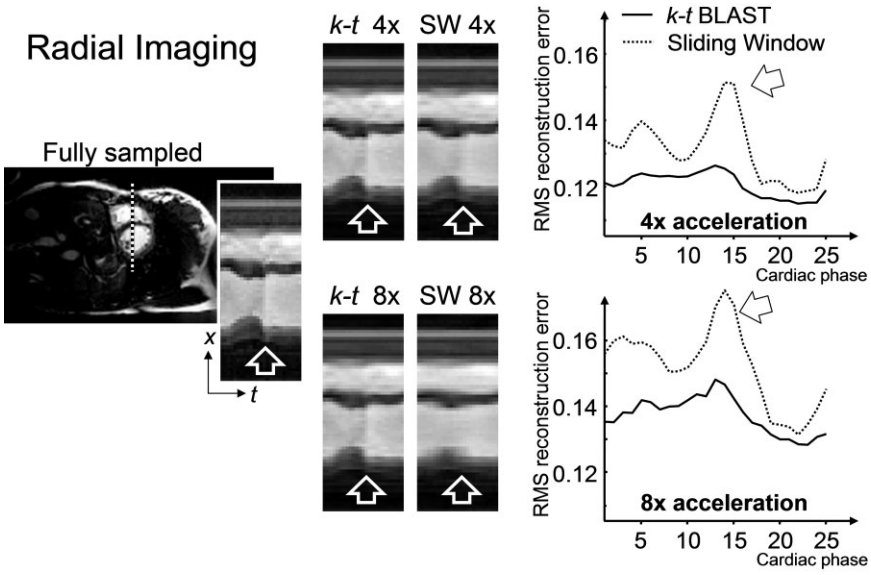

FIG. 4. Reconstruction results for radial imaging. A single frame is shown for full sampling along with an *x-t* plot of the LV. This plot is taken from the position indicated by the dotted line. For four- and eightfold acceleration, only *x-t* plots are shown. The contraction and dilation of the LV are well resolved by the *k-t* BLAST reconstruction, whereas the SW reconstruction introduces blurring. Especially the small jerk at the end of the systole (marked with arrows) is much better preserved by the *k-t* BLAST reconstruction. This is also shown in the RMS reconstruction error plots on the right.

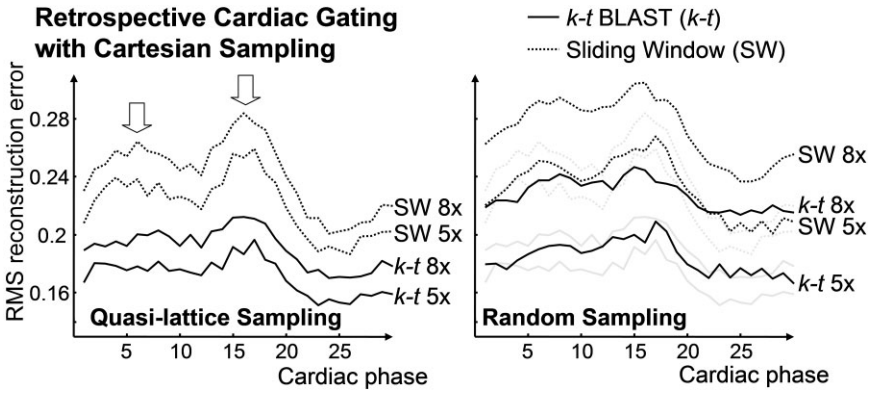

FIG. 5. Reconstruction errors for retrospectively gated Cartesian imaging. The RMS reconstruction error is shown as a function of time (cardiac phase) for five- and eightfold acceleration, for both *k-t* BLAST and SW reconstruction. Quasi-lattice and random sampling patterns were used to generate the left and right graphs, respectively. For comparison, the curves in the left graph are also replicated in gray in the right graph. The arrows indicate cardiac phases with increased error for SW.

For radial imaging, the *k-t* BLAST reconstruction was demonstrated to be superior to the SW reconstruction both visually and quantitatively in terms of the RMS reconstruction error. Furthermore, it was shown that the fully sampled center of *k*-space can be extracted and used as training data in the *k-t* BLAST reconstruction. This makes radial imaging an interesting choice in combination with *k-t* BLAST. Integrating the training into the undersampled acquisition leads to no increase in scan time, as opposed to Cartesian imaging (22). However, the achievable acceleration is limited in this case, since the resolution of the training data is determined by the degree of undersampling. In previous work on the influence of training data quality in Cartesian *k-t* BLAST (19), it was shown that 10–12 training data profiles provided good image quality, although small structures that moved independently of the surrounding tissue (such as small arteries in the lung) benefited from higher-resolution training data. Translating these results to radial imaging, accelerations up to a factor of 10 would be possible for a 128 × 128 matrix.

For retrospectively gated Cartesian imaging, it was shown that the proposed reconstruction is also applicable to a non-regular sampling of the pseudo-time axis. The RMS reconstruction error was lower for the *k-t* BLAST than for the SW reconstruction for both tested undersampling approaches. It turned out that the quasi-lattice undersampling performed better than the random undersampling. This was as expected, since the former minimizes the overlap among signal-bearing regions in *x-f* space. It also points to an advantage of radial or spiral trajectories over arbitrary *k*-space sampling. Although their PSFs are more complicated than in the Cartesian case, they are still localized in *x-f* space, which minimizes signal overlap. Furthermore, the results suggest that the performance of the retrospectively gated *k-t* BLAST acquisitions can be improved if the sampling can be made closer to the opti-

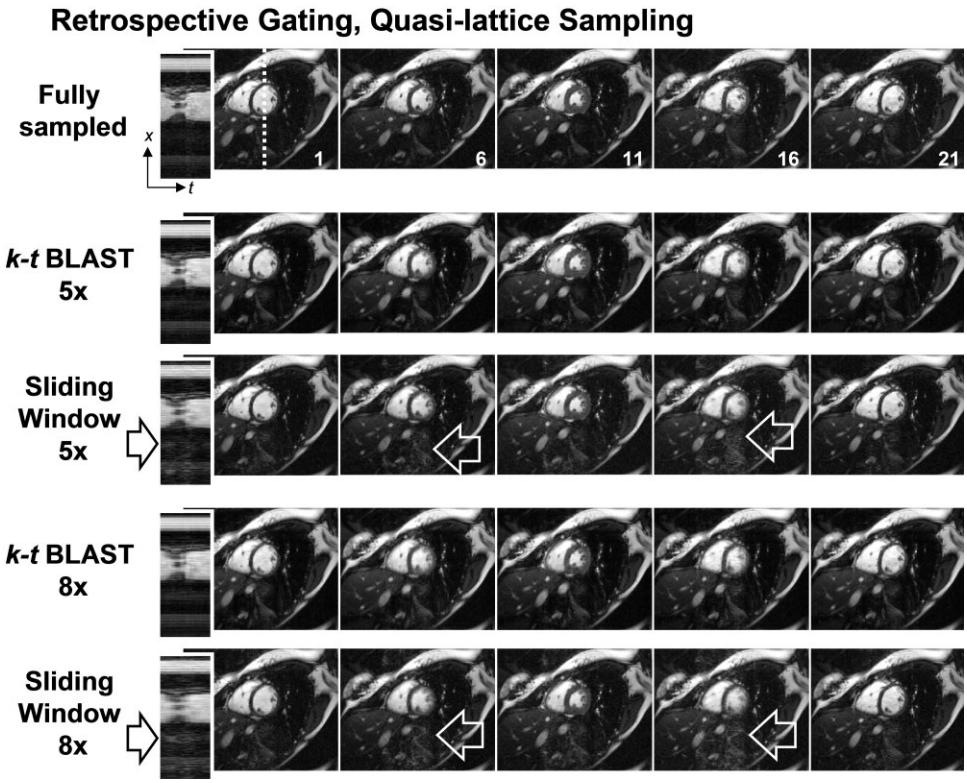

FIG. 6. Example cardiac phases from the retrospectively gated acquisitions using the quasi-lattice undersampling pattern as described in Fig. 2. A reconstruction of the fully sampled data set is depicted in the upper row. The cardiac phase numbers are indicated in the lower right corner of each frame, and an *x-t* plot from a position passing through the LV (indicated with a dotted line) is seen next to the first frame. Rows 2 and 3 show the fivefold-accelerated reconstructions using *k-t* BLAST and SW reconstruction, respectively. The SW reconstructions suffer from residual aliasing artifacts (indicated with arrows) and increased temporal blurring (see *x-t* plots). Similar results are shown for eightfold acceleration in rows 4 and 5.

mal sheared grid by adjusting the sampling during the acquisition based on the ECG. Lattice sampling is generally optimal in terms of minimizing signal overlap in *x-f* space. Nonetheless, reconstruction from non-Cartesian patterns enables the use of important techniques such as retrospective gating and radial or spiral imaging, which offer specific advantages. The optimum choice of the sampling pattern will depend on the application.

In the examples presented here, we chose to stop the iterative reconstruction after 10 iterations. This decision was based on an initial experiment in which the fully sampled data were available and the reconstruction error could be monitored. Normally, the RMS reconstruction error is not known during the reconstruction (since the fully sampled data set is unavailable). It is therefore preferable to use a criterion that is readily available during reconstruction (e.g., one that is based on the residual alone), but it is generally difficult to establish such criteria (23). As previously pointed out in Ref. 15, the residual may not be a reliable measure of convergence. Consequently, it is necessary to run initial convergence experiments for new applications. Our initial experience indicates that the residual has to be reduced by 3–5 orders of magnitude to provide satisfactory reconstruction quality, but this may vary with the application and the acceleration factor used.

The presented RMS reconstruction errors (Figs. 3–5) should be treated with some caution. They are a global measure of differences between the accelerated and non-accelerated cases. Besides residual artifacts, they also represent changes in the distribution of noise in the reconstructed images. The absolute value of the RMS error is of little value for evaluating artifact levels, but it is a useful tool for comparing two methods. The RMS error curves also indicate deviations from the baseline error level, and consequently they can help to identify time frames with more artifacts or blurring. This is indicated with the arrows in Figs. 5 and 6.

The main drawback of the presented method is the reconstruction time required. In the present implementation, the reconstruction time would be on the order of hours for a typical multislice, multicoil cardiac acquisition. However, it would be possible to speed up the reconstruction by at least an order of magnitude with the use of a more efficient implementation (24). This would bring the reconstruction time down to minutes with standard present-day hardware. Furthermore, applications such as the retrospective cardiac gating case require gridding interpolation along only one dimension. Hence, the reconstruction time is considerably shorter for this application.

The presented examples illustrate that the proposed reconstruction is capable of handling applications that do not sample *k-t* space on a lattice. It enables the acceleration provided by *k-t* BLAST to be combined with the specific advantages of alternative sampling strategies. At present, it does not take advantage of the complementary information contained in the data that are simultaneously received by multiple coils. Its extension to *k-t* SENSE will be the subject of future work.

ACKNOWLEDGMENT

M.S.H. acknowledges support from the Danish Heart Foundation (grant #02-2-3-43-22021).

REFERENCES

1. Madore B, Glover GH, Pelc NJ. Unaliasing by Fourier-encoding the overlaps using the temporal dimension (UNFOLD), applied to cardiac imaging and fMRI. Magn Reson Med 1999;42:813–828.
2. Tsao J, Boesiger P, Pruessmann KP. *k-t* BLAST and *k-t* SENSE: dynamic MRI with high frame rate exploiting spatiotemporal correlations. Magn Reson Med 2003;50:1031–1042.
3. Kellman P, Epstein FH, McVeigh ER. Adaptive sensitivity encoding incorporating temporal filtering (TSENSE). Magn Reson Med 2001;45: 846–852.
4. Willis NP, Bresler Y. Optimal scan for time-varying tomography. I. Theoretical analysis and fundamental limitations. IEEE Trans Image Process 1995;4:642–653.
5. Willis NP, Bresler Y. Optimal scan for time-varying tomography. II. Efficient design and experimental validation. IEEE Trans Image Process 1995;4:654–666.
6. Tsao J. On the UNFOLD method. Magn Reson Med 2002;47:202–207.
7. Lenz GW, Haacke EM, White RD. Retrospective cardiac gating: a review of technical aspects and future directions. Magn Reson Imaging 1989; 7:445–455.
8. Barger AV, Block WF, Toropov Y, Grist TM, Mistretta CA. Time-resolved contrast-enhanced imaging with isotropic resolution and broad coverage using an undersampled 3D projection trajectory. Magn Reson Med 2002;48:297–305.
9. Peters DC, Ennis DB, Rohatgi P, Syed MA, McVeigh ER, Arai AE. 3D breath-held cardiac function with projection reconstruction in steady state free precession validated using 2D cine MRI. J Magn Reson Imaging 2004;20:411–416.
10. Scheffler K, Hennig J. Reduced circular field-of-view imaging. Magn Reson Med 1998;40:474–480.
11. Tsao J, Kozerke S, Hansen MS, Eggers H, Boesiger P, Pruessman KP. Moving-buffer *k-t* BLAST for real-time reconstruction: Cartesian and simplified radial cases. In: Proceedings of the 12th Annual Meeting of ISMRM, Kyoto, Japan, 2004. p 635.
12. Pruessmann KP, Weiger M, Scheidegger MB, Boesiger P. SENSE: sensitivity encoding for fast MRI. Magn Reson Med 1999;42:952–962.
13. O'Sullivan J. A fast sinc function gridding algorithm for Fourier inversion in computer tomography. IEEE Trans Med Imaging 1985;MI-4: 200–207.
14. Golub GH, van Loan CF. Matrix computations. 3rd ed. Baltimore: Johns Hopkins University Press; 1996. 520 p.
15. Pruessmann KP, Weiger M, Bornert P, Boesiger P. Advances in sensitivity encoding with arbitrary k-space trajectories. Magn Reson Med 2001;46:638–651.
16. Axelsson O. Iterative solution methods. Cambridge: Cambridge University Press; 1996. 654 p.
17. Peters DC, Korosec FR, Grist TM, Block WF, Holden JE, Vigen KK, Mistretta CA. Undersampled projection reconstruction applied to MR angiography. Magn Reson Med 2000;43:91–101.
18. Roemer PB, Edelstein WA, Hayes CE, Souza SP, Mueller OM. The NMR phased array. Magn Reson Med 1990;16:192–225.
19. Hansen MS, Kozerke S, Pruessmann KP, Boesiger P, Pedersen EM, Tsao J. On the influence of training data quality in *k-t* BLAST reconstruction. Magn Reson Med 2004;52:1175–1183.
20. Tsao J, Kozerke S, Boesiger P, Pruessman KP. Optimizing spatiotemporal sampling for *k-t* BLAST and *k-t* SENSE: application to high-resolution real-time cardiac SSFP. Magn Reson Med 2005;53:1372–1382.
21. Parrish T, Hu X. Continuous update with random encoding (CURE): a new strategy for dynamic imaging. Magn Reson Med 1995;33:326–336.
22. Kozerke S, Tsao J, Razavi R, Boesiger P. Accelerating cardiac cine 3D imaging using *k-t* BLAST. Magn Reson Med 2004;52:19–26.
23. Press PH, Teukolsky SA, Vetterling WT, Flannerly BP. Numerical recipes in C. Cambridge: Cambridge University Press; 1992. 86 p.
24. Eggers H, Boernert P, Boesiger P. Comparison of gridding- and convolution-based iterative reconstruction algorithms for sensitivity-encoded non-Cartesian acquisitions. In: Proceedings of the 10th Annual Meeting of ISMRM, Honolulu, 2002. p 743.